CHEMISTRY OF MATERIALS

pubs.acs.org/cm

Article

In Situ X-Ray Absorption Spectroscopy Disentangles the Roles of Copper and Silver in a Bimetallic Catalyst for the Oxygen Reduction Reaction

Brenna M. Gibbons, Melissa Wette, Michaela Burke Stevens, Ryan C. Davis, Samira Siahrostami, Melissa Kreider, Apurva Mehta,* Drew C. Higgins,* Bruce M. Clemens,* and Thomas F. Jaramillo*

Cite This: *Chem. Mater.* 2020, 32, 1819−1827

Read Online

ACCESS | Metrics & More | Article Recommendations | Supporting Information

ABSTRACT: Silver-based bimetallic catalysts for the oxygen reduction reaction (ORR) are promising for a wide variety of renewable energy technologies, including alkaline fuel cells and metal-air batteries. The activity of bimetallic catalysts can sometimes surpass that of either constituent element, but the origin of the enhanced performance is still debated. At a given active site, two complementary mechanisms are proposed to explain the performance improvements: the binding energy of intermediate adsorbates can be tuned by direct electronic contributions from the alloying element or by changes in the bond lengths from lattice distortion. To distinguish between these effects and elucidate the respective roles of each element in the bimetallic, it is critical to study catalysts at the molecular scale under reaction conditions. In this work, we use in situ X-ray absorption spectroscopy (XAS) alongside density functional theory (DFT) to show that direct electronic rather than geometric effects are the primary cause of improved ORR activity in a bimetallic CuAg catalyst. Our results indicate that the local bonding as well as the electronic structure of Ag are virtually unchanged by the presence of Cu, whereas the electronic states of Cu in CuAg are significantly altered. DFT calculations support these experimental findings. We show strong evidence that the activity of the bimetallic CuAg catalyst exceeds the sum of the activities of Cu and Ag, not by incremental improvement of the active Ag sites, but by creating highly active Cu-centered catalytic sites. The insight that the main role of Ag in bimetallic catalysts may be to promote its fellow element through local electronic interactions provides a new design principle for engineering the next generation of bimetallic catalysts for the ORR and beyond.

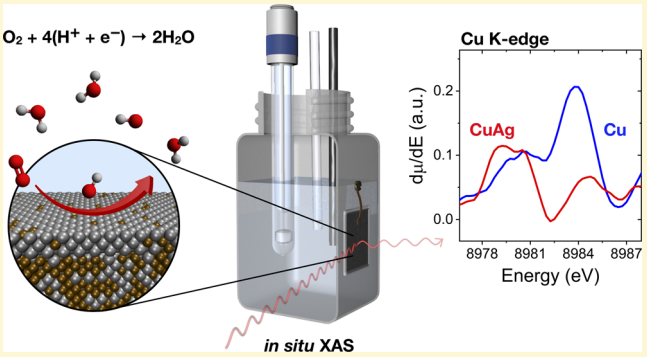

INTRODUCTION

The electrochemical interconversion between oxygen and water is a key process gating the wider deployment of a variety of renewable energy technologies.[1−3] In particular, improving on the kinetics and limited selection of suitable catalysts for the oxygen reduction reaction (ORR) could accelerate the adoption of critical clean-energy technologies such as hydrogen fuel-cell vehicles or metal-air battery-based grid-scale energy storage.[3−6] While Pt-based catalysts are the conventional choice for acidic electrolytes, favorable oxygen reduction kinetics and stability considerations in alkaline electrolytes, as well as recent improvements in anion exchange membranes,[7] provide the possibility for using non-platinum group metal (non-PGM) catalysts.[8,9] Non-PGM options include transition-metal oxides, metal−nitrogen−carbon (M−N−C) systems, and Ag-based catalysts.[8,9] Of these, Ag exhibits important characteristics in terms of conductivity, selectivity, and surface area-normalized turnover frequencies, and it is considered one of few technoeconomically viable alternatives to Pt for the ORR in alkaline conditions.[10]

Although Ag catalysts have achieved high specific activity for a non-PGM material, further improvements are needed to compete with Pt. Nanostructuring can increase the surface area,[11,12] and catalyst loadings of Ag can be much higher than Pt for the same material cost. However, if the catalyst loading is too high, leading to thicker electrodes, these designs may be limited by mass transport. A complementary strategy is to increase the intrinsic activity of Ag catalysts through alloying or mixing with other metals,[13,14] as has been shown for Pt and other catalysts.[15−18] In the well-known Sabatier volcano relationship between the binding energy of an *OH adsorbate and the activity of a metal for the ORR, Ag lies on the weak-

Received: September 26, 2019
Revised: February 5, 2020
Published: February 27, 2020

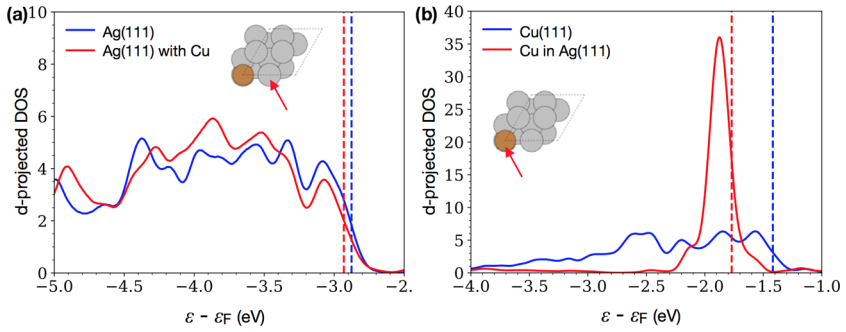

Figure 1. DFT calculations showing the d-projected density of states for (a) a Ag atom in Ag(111) and a Ag atom adjacent to a Cu atom within Ag(111) and (b) a Cu atom in Cu(111) and a Cu atom within Ag(111). While the electronic structure of Ag changes only slightly in the presence of a Cu atom, the density of states of the Cu atom in a Ag lattice is dramatically altered compared to pure Cu. Data from ref 27.

binding side of the volcano. In other words, silver is understood to bind oxygen too weakly, leading to a limiting step of $O_2 + * \rightarrow *O_2^-$.[19,20] An alloy with another metal such as Cu, Co, or Ni could potentially result in a catalyst with a more ideal *OH binding energy and improved catalytic activity.[21,22] However, unlike Pt, Ag does not readily alloy with many of the transition metals. Nonetheless, there have been several bimetallic Ag catalysts reported with increased ORR activity,[23−25] including metastable CoAg nanoparticles for which the activity was attributed to a surface alloy achieved through a rapid heating, rapid quenching technique.[26]

One promising candidate for a mixed Ag−M system is a bimetallic CuAg catalyst, which we showed recently to have improved activity for the ORR in the thin-film form.[27] In that case, physical vapor deposition led to a degree of metastable miscibility between Cu and Ag. The resulting $Cu_{70}Ag_{30}$ catalyst showed a ca. 4-fold activity improvement over pure Ag at an electrode potential of 0.8 V vs reversible hydrogen electrode (RHE) and more than a 30-fold activity improvement at 0.7 V vs RHE. The CuAg catalyst also exhibited electrochemical activity hysteresis, with the forward scan outperforming the reverse scan in a cyclic voltammogram (CV). Density functional theory (DFT) was used to propose two hypotheses for the activity enhancement of CuAg, including (i) the presence of a Ag overlayer on Cu oxide under reaction conditions, leading to tensile strain in the Ag or (ii) Cu atoms in a silver lattice whose d-band structure is dramatically changed compared to pure Cu (see Figure 1). This narrowing of the d-band of Cu has also been predicted by DFT for dilute Cu in Ag and shown experimentally by valence photoemission spectra in another study,[28] although there remains some debate over the effect of this change on the binding energy of oxygen. Bimetallic CuAg is also a promising catalyst for electrochemical CO_2 reduction (CO_2R); the addition of Ag to Cu has been shown to improve the selectivity toward oxygenated multicarbon products.[29−34] Although reaction conditions (electrochemical potentials, pH, electrolyte, etc.) vary between the ORR and CO_2R, understanding the interplay between Ag and Cu under electrochemical conditions is of interest to both communities.

As with any catalyst, to understand the performance of CuAg, it is critical to observe the catalyst surface under reaction conditions. One powerful tool that has proven useful for probing the state of catalysts in situ is X-ray absorption spectroscopy (XAS), which can examine the geometric and electronic states of the atoms in a material as it catalyzes a reaction.[35,36] For Pt and Pd catalysts, for example, tracking the oxidation state of the transition metal over a range of electrochemical potentials and comparing any hysteresis in the oxidation state to the hysteresis seen in cyclic voltammetry of Pt-catalyzed ORR has provided additional insights.[37] Our study takes a similar approach to study the mechanism of improvement in a CuAg catalyst compared to pure Ag by employing in situ XAS.

In this work, we look at both the Ag and Cu absorption edges and identify interesting changes in the redox properties of Cu when it is within a Ag lattice. At ORR-relevant potentials, Cu in the bimetallic system exists in a more metallic state than in a pure Cu catalyst. In addition, we observe similar hysteresis in the oxidation state of Cu as with the hysteresis observed in the electrochemical ORR data. Previous DFT calculations have suggested that the Fermi energy of Cu in a Ag lattice may be dramatically shifted compared to pure Cu, leading to the significant tuning of the binding energy for oxygen.[27] Our experimental findings are consistent, suggesting that Cu in a Ag lattice becomes an additional active site for the ORR and boosts the performance of the bimetallic catalyst despite the poor performance of Cu alone. The strong correlation between theoretical DFT predictions and experimental in situ XAS demonstrates a powerful framework for exploring the mechanistic understanding of electrochemical catalysts.

RESULTS AND DISCUSSION

Improvement in the ORR activity of a thin-film bimetallic CuAg catalyst could, in principle, come from modifications to either the Ag or Cu sites. As Ag alone is significantly more active than Cu alone,[27] it may appear at first glance that modification of the Ag site through strain or electronic effects is the more likely prospect, particularly as the surface of these CuAg catalysts has been shown to be Ag rich after ORR.[27] DFT calculations show little electronic effect on the predicted d-band structure of Ag when modified with dilute amounts of Cu (Figure 1), but our previous calculations predict enhanced activity if Ag is under tensile strain as an overlayer on Cu oxide.[27] Ex situ X-ray diffraction shows a silver-rich phase under compressive strain due to metastable miscibility with Cu, which would appear to refute the tensile strain hypothesis.[27] However, the same study showed Ag enrichment near the surface after electrochemical testing, which may lead to a different Ag environment. To investigate this hypothesis, we deposit thin films (5 nm) of Ag and $Cu_{70}Ag_{30}$ (referred to in this study as CuAg) in a back illumination cell (see the experimental section for more details) and use in situ XAS to

https://dx.doi.org/10.1021/acs.chemmater.9b03963
Chem. Mater. 2020, 32, 1819−1827

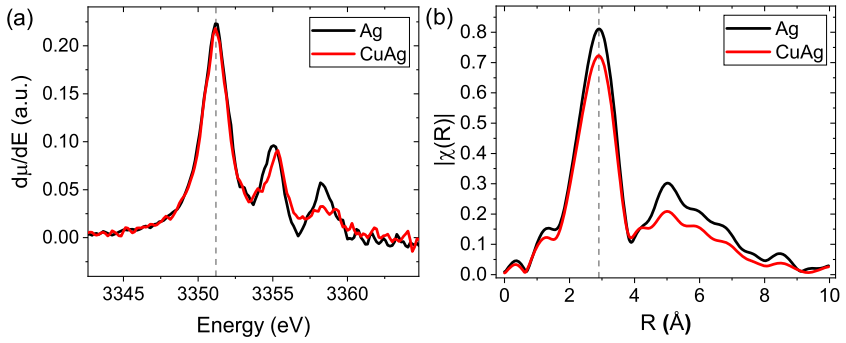

Figure 2. Ag L_3 edge XAS of Ag and CuAg thin films at 0.75 V vs RHE (0.1 M KOH with O_2 bubbling). (a) Derivatives of in situ XANES show that the white line peak (dashed line) is nearly identical in both intensity and position for both compositions. (b) Fourier transforms (FT) of EXAFS show no significant shift of the Ag−Ag distance (dashed line) for Ag and CuAg measured at 0.75 V vs RHE.

probe the electronic and geometric structures of Ag under reaction conditions in 0.1 M KOH. CuAg films with an initial composition of $Cu_{70}Ag_{30}$ have previously been shown to be an optimal composition for ORR activity,[27] as have nanoparticles with an initial composition of $Cu_{75}Ag_{25}$.[24] In both cases, Cu leaches extensively, leaving behind a Ag-rich surface;[24,27] the 5 nm films show a similar Ag enrichment and are therefore used as a template for studying the disperse active sites on the surface. To expand, X-ray photoelectron spectroscopy (XPS) of the 5 nm films post-electrochemical testing indicates Cu near the detection limit (∼0.1%) of the lab-based XPS (see Supporting Information, Figure S3). However, due to the high intensity of the synchrotron radiation, even these low levels of Cu are measurable. The low concentration of Cu after electrochemical testing suggests that under reaction conditions, the Cu sites being measured are near-atomically dispersed. More exact quantification of the ratio of Cu and Ag sites was previously attempted by Pb underpotential deposition,[27,38] but the presence of underpotential deposition stripping features in similar regions for Cu and Ag,[39] as well as background redox features, made the analysis imprecise. We note that with the rise of interest in Ag-based alloy catalysts, there is an opportunity for the development of new techniques to accurately quantify the surface composition of Ag-based alloys.

Comparisons of Ag and CuAg for both X-ray absorption near edge structure (XANES) and extended X-ray absorption fine structure (EXAFS) at the Ag L_3 edge are shown in Figure 2a,b, respectively. In the XANES region, multiple peaks are observed and shift in both intensity and location based on the presence or absence of Cu. The white line peak of Ag, at approximately 3353 eV, is due to the excitation of $2p_{3/2}$ electrons to the first unoccupied levels in Ag, which have a mix of s and d characters. The white line is slightly more intense for CuAg than Ag in the ex situ samples (see Supporting Information, Figure S7), but Ag and CuAg are nearly identical in situ at an electrode potential of 0.75 V vs RHE. Ag is therefore likely slightly more reduced under dry conditions in CuAg, but under ORR conditions there is little if any electronic change. Peaks in the Ag L_3 edge spectra at 3369, 3377, and 3397 eV have been attributed to multiple scattering resonances, which will be affected by the character of the atoms adjacent to Ag. For example, in AgAu bimetallics, these peaks have been shown to shift in both intensity and position because of the influence of Au, which has a similar size as Ag but a different backscattering amplitude and phase.[40,41] In the case of CuAg, these peaks shift in the opposite direction as in AuAg, which is consistent with the trend in backscattering amplitude and atomic weight from Au > Ag > Cu.[42] As these changes in the higher-energy peaks can be attributed to scattering from Cu rather than to the electronic state of the Ag, and the white line of Ag is unchanged in the presence of Cu, it appears that the electronic state of Ag is negligibly changed by the presence of Cu atoms.

To look more closely at the Ag−Ag distances under reaction conditions, the Fourier transform (FT) of the EXAFS is shown in Figure 2b. Though high-resolution EXAFS is impeded by the emergence of the Ag L_2 edge at 3.5237 keV or an approximate wavenumber k of 7 Å, there is a clear single first shell peak at approximately 2.9 Å as well as the extended structure at approximately 5 Å. Under reaction conditions at 0.75 V vs RHE, the location of this peak corresponds to a phase-corrected first shell bond length of 2.86 for both pure Ag and for CuAg (see Table S1 for details). In this case, the FT-EXAFS measurements do not clearly indicate a second peak that could be attributed to a Ag−Cu interaction. However, such a peak may be challenging to observe due to the small k range, low Cu content under reaction conditions, and smaller atomic number of Cu. There does appear to be diminished extended structure in the bimetallic sample, which is likely due to small distortions in the lattice from the presence of Cu. When probed under reaction conditions, Ag L_3 XAS shows no evidence of tensile strain in the first shell of either Ag or CuAg. In neither the XANES nor EXAFS regions of the Ag L_3 edge do there appear to be differences in either the electronic or geometric state of Ag that are significant enough to account for the improved ORR activity observed for the bimetallic catalyst.

If the Ag atoms in CuAg are not changing dramatically, an alternative hypothesis is that the changes in activity are due not to mildly enhanced ORR activity at Ag sites, but to significantly enhanced activity at Cu sites. Although Cu alone is a poor catalyst for the ORR, the dramatic change in the predicted d-band density of states of dilute Cu in Ag (see Figure 1) may lead to correspondingly large changes in activity.[27,28] In one study, the very narrow d-band of Cu in Ag was compared to a free-atom-like state, and the authors posited that the binding energy to oxygen would therefore be increased by 0.3 eV compared to elemental copper using the Newns−Anderson−Grimley model.[28] However, another study predicted that the narrowing of the d-band would be accompanied by a shift in the Fermi energy of Cu by approximately −0.35 eV,[27] corresponding to a more reduced Cu. A similar shift of −0.3 eV has been shown by ex situ XPS and Cu L_3 XAS.[28] As Cu lies on the strong-binding side of the ORR volcano, more reduced Cu should be more active for the ORR.[19,20] To

https://dx.doi.org/10.1021/acs.chemmater.9b03963
Chem. Mater. 2020, 32, 1819−1827

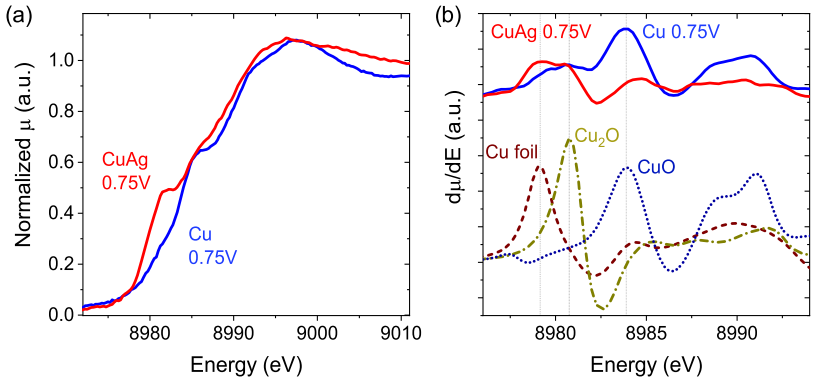

Figure 3. XANES (a) and derivatives (b) of Cu K-edge spectra for a Cu and the CuAg catalyst in situ at 0.75 V vs RHE compared to various copper reference materials. At ORR-relevant conditions, Cu appears to have mostly Cu^{2+} character, while the Cu in CuAg has a mixture of Cu^{0} and Cu^{1+} character.

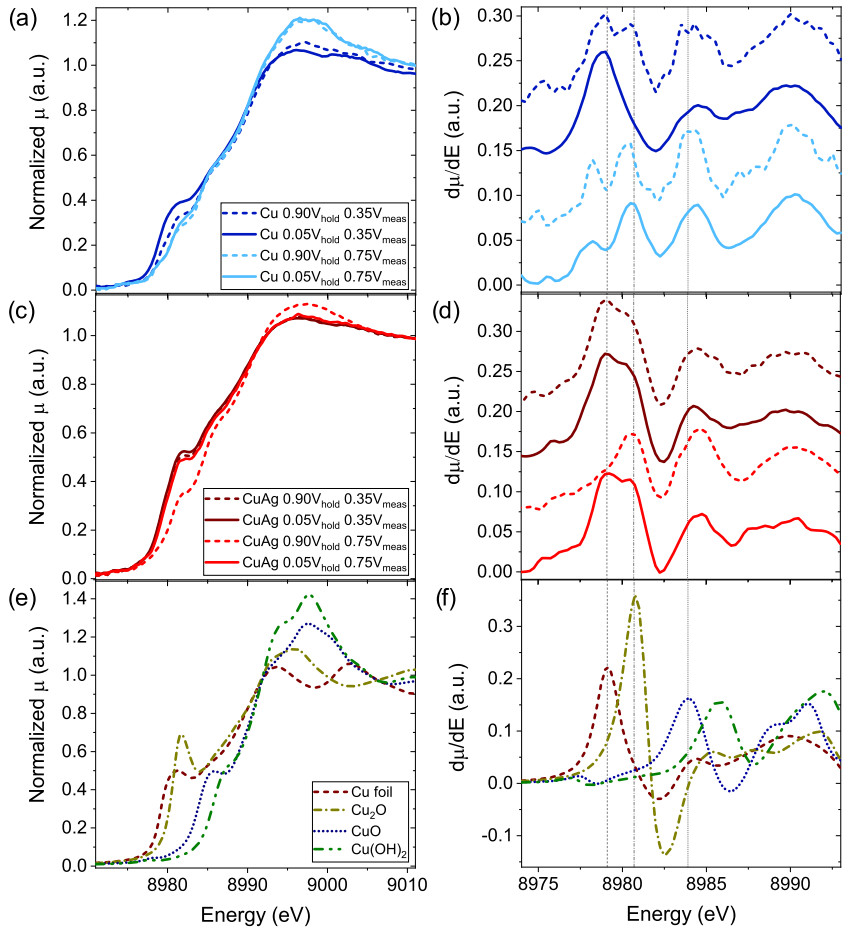

Figure 4. Cu K-edge XANES data (a, c, e) and the corresponding first derivatives of the XANES (b, d, f). (a, b) Cu catalysts in situ at 0.35 and 0.75 V vs RHE. (c, d) CuAg catalysts in situ at 0.35 and 0.75 V vs RHE. (e, f) Reference materials, ex situ. Dashed lines in (b, d, f) highlight the locations of the first peak in the Cu foil, Cu_2O, and CuO XANES derivatives.

resolve the question of the oxygen-binding energy and understand the possible activity changes of Cu in CuAg, we look at the Cu K-edge XAS under reaction conditions.

Figure 3 shows the Cu K-edge spectra collected for both Cu and CuAg. Unlike the Ag L_3 edge spectra, differences at the Cu K-edge are immediately apparent. In Figure 3a, the Cu K-edge XANES spectra of Cu and CuAg are strikingly different when measured at 0.75 V vs RHE, as the edge peak is shifted several eV lower in the CuAg catalyst compared to the pure Cu catalyst. The derivatives of these XANES spectra are plotted in Figure 3b against the derivatives of several known reference materials. Qualitatively, the Cu catalyst measured at 0.75 V vs RHE appears to be most similar to the Cu^{2+} oxide standard, while the Cu in the CuAg catalyst measured at 0.75 V vs RHE appears to be a combination of metallic Cu^{0} and Cu^{1+} oxide. From this qualitative analysis alone, it is clear that Cu exists in a more reduced state under reaction conditions when it occurs in the bimetallic than when it occurs in the pure form. This finding aligns with predictions from DFT that Cu in a silver lattice should have a lower Fermi level and therefore be more

https://dx.doi.org/10.1021/acs.chemmater.9b03963
Chem. Mater. 2020, 32, 1819−1827

reduced under reaction conditions than Cu alone.[27] This calculated change in the Fermi level and the experimental resistance to oxidation of Cu atoms in CuAg compared to pure Cu also suggest that the binding energies of oxygen species to Cu have been weakened, which is consistent with DFT calculations of the binding energy for *O and *OH of 1.39 and 0.64 eV, respectively, for isolated Cu atoms in CuAg and 1.20 and 0.37 eV, respectively, for pure Cu.[19,27] As Cu sits on the strong-binding side of the ORR volcano,[19,20] a decrease in binding energy to oxygen should improve the activity of Cu sites for the ORR.

Because we see no significant changes to the electronic state or bond distance of Ag in the presence of Cu, but we do see drastic shifts in the electronic state of Cu in CuAg compared to pure Cu under reaction conditions, we propose that the enhanced activity of CuAg for the ORR does not arise from an improvement of the Ag site but rather from a new active site at the reduced Cu.

Furthermore, changes in the Cu K-edge XANES spectra of Cu and CuAg as the electrochemical potential is varied support the conclusion that Cu has become the dominant active site for ORR in thin-film CuAg. While the differences at 0.75 V vs RHE, a relevant electrode potential for the ORR, suggest that the improvement in ORR activity originates with Cu rather than Ag, another important feature to understand is the hysteresis seen in the CVs of CuAg.

For each electrochemical potential discussed, XAS spectra were measured under two conditions (see Supporting Information, Figure S5 for schematic). The first is meant to understand phenomena that may occur during the forward sweep of a CV, i.e., toward more positive potentials. This type of measurement involved holding the thin-film catalyst at 0.05 V vs RHE for 5 min before stepping the electrode potential up to the potential of interest, where it was held for the duration of the XAS measurement. This preconditioning is referred to in the Figures and throughout the discussion as a measurement at "0.05 V_{hold}". Similarly, the second type of measurement probes phenomena that may occur during the reverse sweep of a CV, i.e., toward more negative potentials, and consisted of holding the electrode potential at 0.90 V vs RHE before stepping it down to the potential of interest. Measurements taken after this preconditioning step are referred to throughout this work as "0.90 V_{hold}". This procedure was developed to probe the origin of the hysteresis seen in the activity of CuAg for the ORR.

Figure 4 shows the normalized Cu K-edge XANES (a, c, e) and corresponding first derivatives (b, d, f) for a thin-film Cu catalyst in situ (a,b), a thin-film CuAg catalyst in situ (c,d), and reference materials ex situ (e,f). As seen in both Cu and CuAg, the Cu K-edge XANES shows changes in the intensity of the mid-edge peak with the changing electrochemical potential. This is consistent with the presence of Cu redox features in this electrochemical potential window.[27] Evidence of clear changes in the Cu K-edge spectra with response to changing potential also indicates that a significant fraction of the Cu was electrochemically accessible (i.e., near-surface species). For the Cu catalyst, as expected, the in situ XANES spectra become more similar to the oxide standards at more positive electrode potentials; the intensity of the edge peak decreases and the ratio of the first and second peaks in the derivative spectra decreases. For CuAg, the trend is less pronounced due to the greater difference between the 0.05 V_{hold} and 0.90 V_{hold} preconditions, but the fact that we see differences in the XANES with changing electrochemical potential validate the in situ nature of these measurements.

In addition to the simple change of Cu becoming more oxide-like at higher electrode potentials, we see hysteresis in the XANES spectra of Cu for both Cu and CuAg. With the exception of Cu at 0.75 V vs RHE, for which there is little change, the 0.05 V_{hold} measurements (solid lines in Figure 4a−d) are more similar to the Cu foil reference, while the 0.90 V_{hold} measurements (dashed lines in Figure 4a−d) are more similar to the oxide standards. This difference can be clearly seen in the intensity of the first edge peak of the XANES at ∼8981 eV and in the shift of the first peak in the derivative spectra to higher energy. For the Cu catalyst, this difference is most pronounced at 0.35 V vs RHE, while for the CuAg catalyst, the difference is greatest at 0.75 V vs RHE.

To evaluate the Cu K-edge hysteresis more quantitatively, the derivatives of the XANES spectra were fit using linear combination fitting (LCF). $Cu(OH)_2$ did not appear as a contribution to any of the in situ data and is therefore not included. The resulting fits can be viewed as percentage contributions of different Cu species approximated by the reference materials or as an estimate of the average oxidation state, considering that the contribution of the Cu_2O spectra indicates Cu^{1+} character, CuO indicates Cu^{2+} character, and the Cu foil indicates metallic character. LCF analysis of the Cu and CuAg samples measured at 0.75 V vs RHE confirms that the Cu in CuAg is more reduced, with a 47% contribution of metallic-like Cu compared to an 18% contribution for Cu at 0.75 V vs RHE.

Figure 5 shows the results of a LCF analysis of the XANES data for Cu and CuAg at various electrochemical potentials under both the 0.05 V_{hold} (solid) and 0.90 V_{hold} (dashed) conditions. The contribution of the metallic copper standard to the fit is used as the metric of interest because of the hypothesis from DFT that the more reduced Cu has a weaker binding energy for oxygen and will therefore have greater activity for the ORR. As expected, the Cu catalyst loses metallic character at higher electrochemical potentials for both preconditions. However, at lower electrode potentials, the history of the electrode potential the catalyst had seen makes a difference in the measured metallic character; the spectra taken after a reducing electrochemical potential hold show significantly more metallic character than those taken after being held at an oxidizing electrochemical potential. The range of electrochemical potentials for which there is hysteresis in the Cu XAS spectra is consistent with the electrochemical potential range in which the CV of Cu exhibits hysteresis, which confirms the ability of this technique to see the oxidation state changes expected of Cu in this electrochemical potential region.

As seen in the Cu K-edge XANES, Cu and CuAg differ at higher, more ORR-relevant electrode potentials (i.e., above 0.6 vs RHE). For CuAg, hysteresis in the contribution of metallic Cu character is seen at higher potentials. As might be expected, the Cu in CuAg at these potentials is more metallic in character in the 0.05 V_{hold} scan, that is, when the cell was previously held at a reducing potential. When the cell was held at 0.9 V vs RHE and then stepped down to the electrode potential at which the XAS spectra were taken, the Cu in CuAg looks quite similar in metallic character to the Cu in the Cu catalyst. Like Cu, the hysteresis in the contribution of metallic character for CuAg occurs at similar electrode potentials to the hysteresis in the electrochemical activity data. Unlike Cu and

https://dx.doi.org/10.1021/acs.chemmater.9b03963
Chem. Mater. 2020, 32, 1819−1827

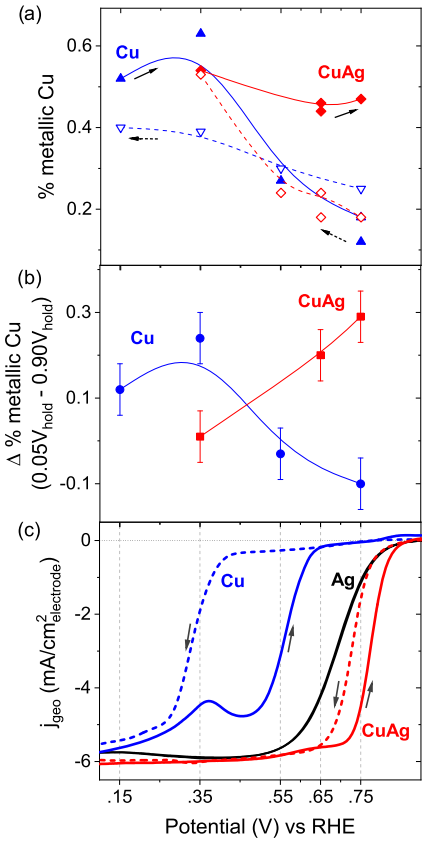

Figure 5. (a) Contribution of a metallic Cu standard to a linear combination fit of in situ Cu K-edge XANES data for Cu and CuAg catalysts. (b) Difference in calculated % metallic character of Cu and CuAg catalysts between 0.05 V_{hold} and 0.90 V_{hold} measurements. (c) Cyclic voltammograms for Cu (blue), Ag (black), and CuAg (red) catalysts. The alignment of the hysteresis in the XAS and electrochemical data suggests that the electronic state of Cu is paramount to its catalytic performance. *CV data from ref 27.

CuAg, Ag shows negligible electrochemical hysteresis (a detail view of Figure 5c can be found in the Supporting Information as Figure S9).

The finding that Cu atoms at more oxidizing potentials (>0.6 V vs RHE) exhibit more metallic character in CuAg than in Cu is consistent with previous results from the CO_2R literature. Previous experimental and theoretical work has speculated that a small electron density donation from Cu to Ag makes the Cu atoms more resistant to oxidation.[43,44] In one case, Ag was not significantly affected because the particles were overall Ag rich and the effect of the donated electrons was therefore diluted.[43] In a similar study of phase-segregated CuAg nanoparticles, the ratio of Cu^0/Cu^{1+} increased as the ratio of Ag/Cu increased, and at low Ag concentrations, a blue-shift in both the XPS binding energies and the characteristic single plasmon resonance (SPR) peak of Ag can be seen that indicates electron density donation from Cu to Ag.[29] However, in situ XAS of the Cu K-edge at −1.2 V vs RHE under CO_2R conditions shows little difference in the electronic state of Cu between pure Cu and either phase-segregated or phase-blended CuAg catalysts,[33] reinforcing that the suppression of Cu oxidation is only relevant at oxidizing conditions (i.e., ex situ in air or at potentials greater than ∼0.6 V vs RHE).

Both previous suggestions that the incorporation of Cu in Ag results in resistance to oxidation and the in situ XAS data shown here are consistent with the second proposed mechanism of improvement from DFT: that rather than a small improvement in the activity of the Ag sites, CuAg has enhanced catalytic activity for the ORR due to a stark increase in the activity of the Cu sites. DFT predicted that dilute Cu in a Ag lattice would have a dramatically different density of states than pure Cu and that it would be significantly reduced as a result.[27] In situ XAS confirms that the Cu in CuAg can and does exist in a more reduced state than in Cu at ORR-relevant electrochemical potentials, indicating a decrease in the binding energy of oxygen species to Cu that should push it closer to the top of the ORR activity volcano. Cu as the dominant active site for the ORR in a bimetallic CuAg catalyst can explain both the improved performance of CuAg compared to Ag and the hysteresis seen in the CuAg electrochemistry, which improves our confidence in this hypothesis, as does the strong correlation between DFT and experimental in situ characterization.

CONCLUSIONS

The incorporation of a Cu atom into a Ag lattice is predicted by DFT to significantly change its Fermi level and therefore its binding energy for ORR intermediates. Under ORR conditions, the Ag atoms in a thin-film CuAg catalyst have a nearly identical L_3-edge white line peak and Ag−Ag distance as pure Ag, while the Cu atoms in a CuAg catalyst are significantly more metallic in character when in the presence of Ag. We therefore conclude that the effect of Ag changing the electronic state of Cu is more potent in this case than the geometric or electronic effect of Cu atoms on the Ag lattice.

In situ XAS of catalyst materials during electrochemical reactions has proven to be a powerful tool for differentiating the role of each element in a bimetallic catalyst, particularly when combined with DFT. Even without directly viewing the adsorbate interactions in situ XAS provides compelling evidence that Cu has surpassed the performance of pure Ag and likely become the dominant active site for CuAg, despite the poor ORR activity of Cu alone. This work not only provides insights into the interaction between Cu and Ag that may be useful for reactions beyond the ORR; it also suggests a possible design principle for future nonprecious ORR catalysts. Based on the CuAg system, we anticipate that other alloys in which the d-band structure is significantly narrowed and shifted may be promising candidates for much sought after catalytically competitive, cheap, stable, and earth-abundant catalysts.

EXPERIMENTAL SECTION

Computational Details. Simulations were performed using the atomic simulation environment (ASE),[45] and electronic structure calculations were performed using the Quantum ESPRESSO program.[46] For further details, refer to ref 27.

Experimental Details. All XAS measurements were performed at Stanford Synchrotron Radiation Lightsource (SSRL) at SLAC National Laboratory in California. Ag L-edge XAS used beamline 14-3a, a tender X-ray beamline with a Si(111) monochromator in the ϕ = 90° setting, and a 4-element Vortex detector to detect fluorescence. The intensity of the incoming beam was measured using ion chambers. Cu K-edge measurements were conducted at beamlines 4-1 and 11-2. 4-1 and 11-2 are both hard X-ray beamlines with an LN_2-cooled Si(220) monochromator used in the ϕ = 90 position. At 4-1, a Canberra 30-element Ge solid-state detector was used, and a similar 100-element detector was used at 11-2. All XAS data were processed using SixPack[47] and Athena.[48]

https://dx.doi.org/10.1021/acs.chemmater.9b03963
Chem. Mater. 2020, 32, 1819−1827

Ag, Cu, and CuAg thin films (5 nm) were deposited by electron beam evaporation in a custom physical vapor deposition system (Technical Engineering Services) as previously described.[27] The substrate was an 8 μm thick Kapton film (DuPont) pyrolyzed at 1000 °C for 1 h in N_2, following the procedure from ref 49. A 2 nm Ti sticking layer, deposited in the same system, was used for the Cu and CuAg samples to increase adhesion. In addition to our pure Cu and pure Ag reference films, we used a $Cu_{70}Ag_{30}$ film, as this composition was the most active for the ORR in our previous study.[27]

All experiments were done using an in situ back illumination cell to maximize the signal at the lower energy Ag L-edge. Schematics and pictures of the cell can be found in the supporting information, Figure S2. The cell was constructed from a 50 mL high-density polyethylene (HD-PE, Nalgene) bottle. The electrolyte was 0.1 M KOH prepared from semiconductor grade pellets (Sigma-Aldrich) and Millipore water (R = 10 MΩ·cm). The counter electrode, a graphite rod (Ted Pella), and a Ag/AgCl 4M KCl reference electrode (Fisher Scientific, Accumet) were inserted through the mouth of the bottle. Oxygen was bubbled through a glass frit for the duration of the experiment. The working electrode of the metal on pyrolyzed Kapton was epoxied over a 0.67 cm diameter hole in the cell wall and contacted with a copper clip (Ted Pella). For measurements at the Ag L-edge, the entire cell was enclosed in a box purged with He to minimize scatter loss in air.

Electrochemical data during the in situ experiments were conducted using a Biologic SP-300 potentiostat. All electrode potentials are reported vs the reversible hydrogen electrode (RHE) based on a calibration of the Ag/AgCl electrode vs a clean Pt wire in the H_2-saturated 0.1 M KOH electrolyte. For each new sample, an initial CV was run from 0.05 to 0.9 V vs RHE. For each XAS measurement, the sample was first polarized at either 0.05 V vs RHE (0.05 V_{hold} conditions) or 0.9 V vs RHE (0.90 V_{hold} conditions) for 5 min before being brought to the electrochemical potential of interest where it was held for the duration of the measurement (see Supporting Information, Figure S5).

■ ASSOCIATED CONTENT

Supporting Information

The Supporting Information is available free of charge at https://pubs.acs.org/doi/10.1021/acs.chemmater.9b03963.

Computational details, experimental setup details, supplementary experimental characterization (SEM and XPS), and additional XAS data and fitting (PDF)

Raw data from all main text figures are also provided, in line with the U.S. Department of Energy requirements (XSLX)

■ AUTHOR INFORMATION

Corresponding Authors

Apurva Mehta − *SLAC National Accelerator Laboratory, Menlo Park, California 94025, United States;* orcid.org/0000-0003-0870-6932; Email: mehta@slac.stanford.edu

Drew C. Higgins − *Department of Materials Science, Stanford University, Stanford, California 94035, United States; Department of Chemical Engineering, McMaster University, Hamilton, Ontario L8S 4L8, Canada;* orcid.org/0000-0002-0585-2670; Email: dhiggins@mcmaster.ca

Bruce M. Clemens − *Department of Materials Science, Stanford University, Stanford, California 94035, United States;* Email: bmc@stanford.edu

Thomas F. Jaramillo − *Department of Chemical Engineering, Stanford University, Stanford, California 94035, United States;* orcid.org/0000-0001-9900-0622; Email: jaramillo@stanford.edu

Authors

Brenna M. Gibbons − *Department of Materials Science, Stanford University, Stanford, California 94035, United States*

Melissa Wette − *Department of Materials Science, Stanford University, Stanford, California 94035, United States;* orcid.org/0000-0002-7127-1751

Michaela Burke Stevens − *Department of Chemical Engineering, Stanford University, Stanford, California 94035, United States;* orcid.org/0000-0003-3584-0600

Ryan C. Davis − *SLAC National Accelerator Laboratory, Menlo Park, California 94025, United States*

Samira Siahrostami − *Department of Chemistry, University of Calgary, Calgary, Alberta T2N 1N4, Canada;* orcid.org/0000-0002-1192-4634

Melissa Kreider − *Department of Chemical Engineering, Stanford University, Stanford, California 94035, United States;* orcid.org/0000-0003-1750-6860

Complete contact information is available at: https://pubs.acs.org/10.1021/acs.chemmater.9b03963

Notes

The authors declare no competing financial interest.

■ ACKNOWLEDGMENTS

The authors gratefully acknowledge the Toyota Research Institute for support of experimental and computational work. The U.S. Department of Energy, Office of Basic Energy Sciences, Chemical Sciences, Geosciences, and Biosciences Division, Catalysis Science Program is gratefully acknowledged for primary support for SUNCAT Center for Interface Science and Catalysis. The use of the Stanford Synchrotron Radiation Lightsource, SLAC National Accelerator Laboratory, is supported by the U.S. Department of Energy, Office of Science, Office of Basic Energy Sciences under Contract No. DE-AC02-76SF00515. Part of this work was performed at the Stanford Nano Shared Facilities (SNSF), supported by the National Science Foundation under award ECCS-1542152. B.M.G. acknowledges support from the U.S. Department of Defense through the National Defense Science and Engineering Graduate Fellowship. B.M.G., M.B.S., and M.E.K. acknowledge support from the Toyota Research Institute. S.S. acknowledges the support from the University of Calgary's Canada First Research Excellence Fund Program, the Global Research Initiative in Sustainable Low Carbon Unconventional Resources. D.C.H. acknowledges support from the Banting Postdoctoral Fellowship program, administered by the Government of Canada. The authors thank Jakob Kibsgaard for help with 3D image modeling. The authors used VMD for part of the TOC image.[50,51]

■ REFERENCES

(1) Stamenkovic, V. R.; Strmcnik, D.; Lopes, P. P.; Markovic, N. M. Energy and Fuels from Electrochemical Interfaces. *Nat. Mater.* **2017**, *16*, 57−69.

(2) Chen, Z.; Higgins, D.; Yu, A.; Zhang, L.; Zhang, J. A Review on Non-precious Metal Electrocatalysts for PEM. *Energy Environ. Sci.* **2011**, *4*, 3167−3192.

(3) Debe, M. K. Electrocatalyst Approaches and Challenges for Automotive Fuel Cells. *Nature* **2012**, *486*, 43−51.

(4) Ramaswamy, N.; Mukerjee, S. Fundamental Mechanistic Understanding of Electrocatalysis of Oxygen Reduction on Pt and Non-Pt Surfaces: Acid versus Alkaline Media. *Adv. Phys. Chem.* **2012**, *2012*, 1−17.

(5) Jensen, K. D.; Tymoczko, J.; Rossmeisl, J.; Bandarenka, A. S.; Chorkendorff, I.; Escudero-Escribano, M.; Stephens, I. E. L. Elucidation of the Oxygen Reduction Volcano in Alkaline Media using a Copper-Platinum(111) Alloy. *Angew. Chem., Int. Ed.* **2018**, *57*, 2800−2805.
(6) Posada, J. O. G.; Rennie, A. J.; Villar, S. P.; Martins, V. L.; Marinaccio, J.; Barnes, A.; Glover, C. F.; Worsley, D. A.; Hall, P. J. Aqueous Batteries as Grid Scale Energy Storage Solutions. *Renewable Sustainable Energy Rev.* **2017**, *68*, 1174−1182.
(7) Dekel, D. R. Review of Cell Performance in Anion Exchange Membrane Fuel Cells. *J. Power Sources* **2018**, *375*, 158−169.
(8) Ge, X.; Sumboja, A.; Wuu, D.; An, T.; Li, B.; Goh, F. W.; Hor, T. S.; Zong, Y.; Liu, Z. Oxygen Reduction in Alkaline Media: From Mechanisms to Recent Advances of Catalysts. *ACS Catal.* **2015**, *5*, 4643−4667.
(9) Nie, Y.; Li, L.; Wei, Z. Recent Advancements in Pt and Pt-free Catalysts for Oxygen Reduction Reaction. *Chem. Soc. Rev.* **2015**, *44*, 2168−2201.
(10) Setzler, B. P.; Zhuang, Z.; Wittkopf, J. A.; Yan, Y. Activity Targets for Nanostructured Platinum-Group-Metal-Free Catalysts in Hydroxide Exchange Membrane Fuel Cells. *Nat. Nanotechnol.* **2016**, *11*, 1020−1025.
(11) Ohyama, J.; Okata, Y.; Watabe, N.; Katagiri, M.; Nakamura, A.; Arikawa, H.; Shimizu, K.-i.; Takeguchi, T.; Ueda, W.; Satsuma, A. Oxygen Reduction Reaction Over Silver Particles with Various Morphologies and Surface Chemical States. *J. Power Sources* **2014**, *245*, 998−1004.
(12) Garlyyev, B.; Liang, Y.; Butt, F. K.; Bandarenka, A. S. Engineering of Highly Active Silver Nanoparticles for Oxygen Electroreduction via Simultaneous Control over Their Shape and Size. *Adv. Sustainable Syst.* **2017**, *1*, No. 1700117.
(13) Erikson, H.; Sarapuu, A.; Tammeveski, K. Oxygen Reduction Reaction on Silver Catalysts in Alkaline Media: a Minireview. *ChemElectroChem* **2019**, *6*, 73−86.
(14) Qaseem, A.; Chen, F.; Wu, X.; Johnston, R. L. Pt-Free Silver Nanoalloy Electrocatalysts for Oxygen Reduction Reaction in Alkaline Media. *Catal. Sci. Technol.* **2016**, *6*, 3317−3340.
(15) Stamenkovic, V. R.; Mun, B. S.; Arenz, M.; Mayrhofer, K. J.; Lucas, C. A.; Wang, G.; Ross, P. N.; Markovic, N. M. Trends in Electrocatalysis on Extended and Nanoscale Pt-Bimetallic Alloy Surfaces. *Nat. Mater.s* **2007**, *6*, 241−247.
(16) Escudero-Escribano, M.; Malacrida, P.; Hansen, M. H.; Vej-Hansen, U. G.; Velázquez-Palenzuela, A.; Tripkovic, V.; Schiøtz, J.; Rossmeisl, J.; Stephens, I. E.; Chorkendorff, I. Tuning the Activity of Pt Alloy Electrocatalysts by Means of the Lanthanide Contraction. *Science* **2016**, *352*, 73−76.
(17) Toda, T.; Igarashi, H.; Uchida, H.; Watanabe, M. Enhancement of the Electroreduction of Oxygen on Pt Alloys with Fe, Ni, and Co. *J. Electrochem. Soc.* **1999**, *146*, No. 3750.
(18) Mukerjee, S. Role of Structural and Electronic Properties of Pt and Pt Alloys on Electrocatalysis of Oxygen Reduction. *J. Electrochem. Soc.* **1995**, *142*, No. 1409.
(19) Nørskov, J. K.; Rossmeisl, J.; Logadottir, A.; Lindqvist, L.; Kitchin, J. R.; Bligaard, T.; Jónsson, H. Origin of the Overpotential for Oxygen Reduction at a Fuel-Cell Cathode. *J. Phys. Chem. B* **2004**, *108*, 17886−17892.
(20) Kulkarni, A.; Siahrostami, S.; Patel, A.; Nørskov, J. K. Understanding Catalytic Activity Trends in the Oxygen Reduction Reaction. *Chem. Rev.* **2018**, *118*, 2302−2312.
(21) Stamenkovic, V.; Mun, B. S.; Mayrhofer, K. J.; Ross, P. N.; Markovic, N. M.; Rossmeisl, J.; Greeley, J.; Nørskov, J. K. Changing the Activity of Electrocatalysts for Oxygen Reduction by Tuning the Surface Electronic Structure. *Angew. Chem., Int. Ed.* **2006**, *45*, 2897−2901.
(22) Medford, A. J.; Vojvodic, A.; Hummelshøj, J. S.; Voss, J.; Abild-Pedersen, F.; Studt, F.; Bligaard, T.; Nilsson, A.; Nørskov, J. K. From the Sabatier Principle to a Predictive Theory of Transition-Metal Heterogeneous Catalysis. *J. Catal.* **2015**, *328*, 36−42.
(23) Song, X.; Zhang, D. Bimetallic Ag−Ni/C Particles as Cathode Catalyst in AFCs (Alkaline Fuel Cells). *Energy* **2014**, *70*, 223−230.
(24) Wu, X.; Chen, F.; Zhang, N.; Qaseem, A.; Johnston, R. L. Engineering Bimetallic Ag-Cu Nanoalloys for Highly Efficient Oxygen Reduction Catalysts: A Guideline for Designing Ag-Based Electrocatalysts with Activity Comparable to Pt/C-20%. *Small* **2017**, *13*, No. 1603876.
(25) Zhang, N.; Chen, F.; et al. The Activity Origin of Core-Shell and Alloy AgCu Bimetallic Nanoparticles for the Oxygen Reduction Reaction. *J. Mater. Chem. A* **2017**, *5*, 7043−7054.
(26) Holewinski, A.; Idrobo, J. C.; Linic, S. High-Performance Ag-Co Alloy Catalysts for Electrochemical Oxygen Reduction. *Nat. Chem.* **2014**, *6*, 828−834.
(27) Higgins, D.; Wette, M.; Gibbons, B. M.; Siahrostami, S.; Hahn, C.; Escudero-Escribano, M.; García-Melchor, M.; Ulissi, Z.; Davis, R. C.; Mehta, A.; Clemens, B. M.; Nørskov, J. K.; Jaramillo, T. F. Copper Silver Thin Films with Metastable Miscibility for Oxygen Reduction Electrocatalysis in Alkaline Electrolytes. *ACS Appl. Energy Mater.* **2018**, *1*, 1990−1999.
(28) Greiner, M. T.; Jones, T. E.; Beeg, S.; Zwiener, L.; Scherzer, M.; Girgsdies, F.; Piccinin, S.; Armbrüster, M.; Knop-Gericke, A.; Schlögl, R. Free-Atom-Like d States in Single-Atom Alloy catalysts. *Nat. Chemistry* **2018**, *10*, 1008−1015.
(29) Mantella, V.; Oveisi, E.; Mensi, M.; Huang, J.; Buonsanti, R. Structural Sensitivities in Bimetallic Catalysts for Electrochemical CO2 Reduction Revealed by Ag-Cu Nanodimers. *J. Am. Chem. Soc.* **2019**, *141*, 2490−2499.
(30) Higgins, D.; Landers, A. T.; Ji, Y.; Nitopi, S.; Morales-Guio, C. G.; Wang, L.; Chan, K.; Hahn, C.; Jaramillo, T. F. Guiding Electrochemical Carbon Dioxide Reduction toward Carbonyls Using Copper Silver Thin Films with Interphase Miscibility. *ACS Energy Lett.* **2018**, *3*, 2947−2955.
(31) Hoang, T. T.; Verma, S.; Ma, S.; Fister, T. T.; Timoshenko, J.; Frenkel, A. I.; Kenis, P. J.; Gewirth, A. A. Nanoporous Copper-Silver Alloys by Additive-Controlled Electrodeposition for the Selective Electroreduction of CO2 to Ethylene and Ethanol. *J. Am. Chem. Soc.* **2018**, *140*, 5791−5797.
(32) Clark, E. L.; Hahn, C.; Jaramillo, T. F.; Bell, A. T. Electrochemical CO2 Reduction over Compressively Strained CuAg Surface Alloys with Enhanced Multi-Carbon Oxygenate Selectivity. *J. Am. Chem. Soc.* **2017**, *139*, 15848−15857.
(33) Lee, S.; Park, G.; Lee, J. Importance of Ag-Cu Biphasic Boundaries for Selective Electrochemical Reduction of CO2 to Ethanol. *ACS Catal.* **2017**, *7*, 8594−8604.
(34) Wang, D.; Meyer, T. J.; Sheridan, M. V.; Wang, Y.; Dares, C. J.; Marquard, S. L. CO2 Reduction to Acetate in Mixtures of Ultrasmall (Cu)n, (Ag)m Bimetallic Nanoparticles. *Proc. Natl. Acad. Sci. U.S.A.* **2017**, *115*, 278−283.
(35) Russell, A. E.; Rose, A. X-ray Absorption Spectroscopy of Low Temperature Fuel Cell Catalysts. *Chem. Rev.* **2004**, *104*, 4613−4635.
(36) Kumar, M.; Deka, S. Multiply Twinned AgNi Alloy Nanoparticles as Highly Active Catalyst for Multiple Reduction and Degradation Reactions. *ACS Appl. Mater. Interfaces* **2014**, *6*, 16071−16081.
(37) Nagamatsu, S. I.; Arai, T.; Yamamoto, M.; Ohkura, T.; Oyanagi, H.; Ishizaka, T.; Kawanami, H.; Uruga, T.; Tada, M.; Iwasawa, Y. Potential-Dependent Restructuring and Hysteresis in the Structural and Electronic Transformations of Pt/C, Au(Core)-Pt(Shell)/C, and Pd(Core)-Pt(Shell)/C Cathode Catalysts in Polymer Electrolyte Fuel Cells Characterized by in situ X-ray Absorption Fine Structure. *J. Phys. Chem. C* **2013**, *117*, 13094−13107.
(38) Herrero, E.; Buller, L. J.; Abruña, H. D. Underpotential Deposition at Single Crystal Surfaces of Au, Pt, Ag and Other Materials. *Chem. Rev.* **2001**, *101*, 1897−1930.
(39) Brisard, G. M.; Zenati, E.; Gasteiger, H. A.; Markovic, N.; Ross, P. N. Underpotential Deposition of Lead on Copper(111): A Study Using a Single-Crystal Rotating Ring Disk Electrode and ex Situ Low-Energy Electron Diffraction and Scanning tunneling Microscopy. *Langmuir* **1995**, *11*, 2221−2230.

(40) Kozachuk, M.; Martin, R.; Sham, T.; Robinson, M.; Nelson, A. The Application of XANES for the Examination of Silver, Gold, Mercury, and Sulfur on the Daguerreotype Surface. *Can. J. Chem.* **2017**, *95*, 1156−1162.
(41) Bzowski, A.; Sham, T. K.; Yiu, Y. M. Ag L-edge X-ray-Absorption Near-Edge-Structure Study of Charge Redistribution at the Ag Site in Au-Ag Alloys. *Phys. Rev. B* **1994**, *49*, 13776−13779.
(42) Yano, J.; Yachandra, V. K. X-ray Absorption Spectroscopy. *Photosynth. Res.* **2009**, *102*, 241−254.
(43) Kim, N. R.; Shin, K.; Jung, I.; Shim, M.; Lee, H. M. Ag-Cu Bimetallic Nanoparticles with Enhanced Resistance to Oxidation: A Combined Experimental and Theoretical Study. *J. Phys. Chem. C* **2014**, *118*, 26324−26331.
(44) Chen, Z.; Mochizuki, D.; Maitani, M. M.; Wada, Y. Facile Synthesis of Bimetallic Cu-Ag Nanoparticles Under Microwave Irradiation and Their Oxidation Resistance. *Nanotechnology* **2013**, *24*, No. 265602.
(45) Bahn, S.; Jacobsen, K. An Object-Oriented Scripting Interface to a Legacy Electronic Structure Code. *Comput. Sci. Eng.* **2002**, *4*, 56−66.
(46) Giannozzi, P.; et al. QUANTUM ESPRESSO: a Modular and Open-Source Software Project for Quantum Simulations of Materials. *J. Phys.: Condens. Matter* **2009**, *21*, No. 395502.
(47) Webb, S. M. SIXPack a Graphical User Interface for XAS Analysis Using IFEFFIT. *Phys. Scr.* **2005**, *2005*, No. 1011.
(48) Ravel, B.; Newville, M. ATHENA, ARTEMIS, HEPHAESTUS: Data Analysis for X-ray Absorption Spectroscopy Using IFEFFIT. *J. Synchrotron Radiat.* **2005**, *12*, 537−541.
(49) Pedersen, A. F. Elucidating Oxygen Electrocatalysis with Synchrotron X-rays: PEM Fuel Cells and Electrolyzers. Ph.D. Thesis, Technical University of Denmark: Kongens Lyngby, Denmark, 2016.
(50) Humphrey, W.; Dalke, A.; Schulten, K. VMD—Visual Molecular Dynamics. *J. Mol. Graphics* **1996**, *14*, 33−38.
(51) Stone, J. An Efficient Library for Parallel Ray Tracing and Animation. M.Sc. Thesis, University of Missouri-Rolla, 1998.

https://dx.doi.org/10.1021/acs.chemmater.9b03963
Chem. Mater. 2020, 32, 1819−1827